Heliyon 9 (2023) e17526

Contents lists available at ScienceDirect

Heliyon

journal homepage: www.cell.com/heliyon

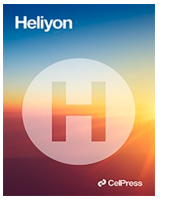

Evaluation indices of the temperature difference of subgrade and the optimization of mitigation measures in cold regions

Yu-zhi Zhang [a,b,*], Xiao-jie Liang [c,d], Ya-qian Dong [d], Cheng-yan Li [d], Zhi-rong Zhao [e,**]

[a] *Key Laboratory for Health Monitoring and Control of Large Structures in Hebei Province, Shijiazhuang Tiedao University, Shijiazhuang 050043, China*
[b] *Collaborative Innovation Center for Performance and Safety of Large-scale Infrastructure, Shijiazhuang Tiedao University, Shijiazhuang 050043, China*
[c] *China Railway Sixth Bureau Group, Shijiazhuang Railway Construction Co., Ltd., Shijiazhuang, 050010, China*
[d] *School of Civil Engineering, Shijiazhuang Tiedao University, Shijiazhuang 050043, China*
[e] *Shuohuang Railway Development Co., Ltd., Suning 062350, China*

ARTICLE INFO

Keywords:
Transverse ground temperature difference
Homogeneity index
Symmetry index
Mitigation measure
Insulation material

ABSTRACT

With the construction and operation of railways in cold regions, the asymmetric deformation of subgrades due to the difference in the transverse ground temperature has become a prominent issue. A comprehensive evaluation of the transverse ground temperature difference and investigation of the corresponding mitigation measures should be conducted to avoid or minimize the damage resulting from this difference, thereby improving subgrade stability and reducing deformation. In this study, the time history variations in the homogeneity and symmetry indices of the ground temperature at typical instances that reflect the spatial and temporal changes in the temperature difference of the subgrade were proposed as evaluation indices. The feasibility of these evaluation indices was verified through numerical models with different types of anti-frost berms. Subsequently, the numerical models were used to analyze the ground temperature evaluation indices of a subgrade with expanded polystyrene (EPS) insulation board and polyurethane (PU) insulation board at different locations. Additionally, the performances of each mitigation measure in eliminating or reducing the ground temperature difference were assessed and compared. The results show that all the mitigation measures could improve the homogeneity and symmetry of the ground temperature distribution. The maximum mitigation rates for the homogeneity and symmetry are 97.87% and 45.90%, respectively. This study provides a comprehensive evaluation method for the temperature difference of subgrades constructed in cold regions and a theoretical reference for the selection of anti-frost measures in the design, operation, and maintenance of subgrades in cold regions.

* Corresponding author. Key Laboratory for Health Monitoring and Control of Large Structures in Hebei Province, Shijiazhuang Tiedao University, Shijiazhuang 050043, China.
** Corresponding author. No. 17 East Beierhuan Rd., Shijiazhuang, Hebei, 050043, China.
E-mail addresses: zhangyuzhi@stdu.edu.cn (Y.-z. Zhang), 36177254@qq.com (Z.-r. Zhao).

https://doi.org/10.1016/j.heliyon.2023.e17526
Received 27 December 2022; Received in revised form 22 May 2023; Accepted 20 June 2023
Available online 28 June 2023

1. Introduction

In China, nearly one-fourth of the land is covered by permafrost, and more than half of the land is seasonally frozen. With the development of China's economy, the demand for high-speed railways (HSRs) is increasing. The construction of HSRs in cold regions, such as the Harbin–Dalian Railway and Harbin–Qiqihar Railway, is inevitably associated with the phenomenon of subgrade frost heave [1–6]. If unaddressed, the frost heave would significantly affect the ride comfort and operational safety of trains.

The Harbin–Dalian Railway, which is constructed in a deep seasonally frozen region, has a ballastless track and is the first HSR in cold regions. The seasonally frozen layer along the railway is quite thick, with the frost depth ranging from 1.40 to 2.05 m, and the frozen time is relatively long. The measured data and transient numerical model results of the subgrade in the Harbin–Dalian Railway show that HSR construction, difference in solar radiation, and route direction induce a heat imbalance on both sides of the subgrade, resulting in different ground temperatures in the transverse section [1,5–8]. Niu et al. [1] monitored the ground temperature of a typical roadbed–culvert transition section of the Harbin–Dalian Railway. The results showed that in cold seasons, the sunny-shady slope effect results in a shallow ground temperature difference of 2.5 °C under the railway shoulder. For the same cross section, as the depth increases, the influence of ground temperature difference gradually reduces. Based on the monitored ground temperature of the subgrade in the Harbin–Dalian Railway, Zhang et al. [7] confirmed the existence of transverse ground temperature difference, and the latitude and subgrade height were found to affect the differences in subgrade sections. A coupling calculation of the temperature and deformation fields of a subgrade [8] revealed that it exhibited transverse deformation difference and that tensile cracks were likely to occur in the shoulder and slope of the subgrade. Zhang et al. [6,9] investigated the features of the spatiotemporal changes in the subgrade deformation and ground temperature in the Harbin–Dalian Railway. The analysis of the time histories of the ground temperatures at different positions in four different subgrade cross sections revealed that in the sunny and shady slopes with the same depth of different cross sections, the ground temperature difference fluctuated between 0 °C and 6 °C. The heat in the subgrade transferred mainly from top to bottom, leading to a delayed ground temperature response, and the average ground temperature differences in the hottest and coldest months in both the subgrade shoulders do not disappear with the depth but form a spindle shape beneath the subgrade.

To date, however, there is a lack of research on subgrade deformation difference due to transverse ground temperature differences in seasonally frozen regions. In railway construction, there are strict requirements on the smoothness and safety of railways, particularly in the case of HSRs. Currently, significant efforts have been made to clarify the transverse ground temperature difference in subgrades of road and railway in permafrost regions, including the proposal of corresponding mitigation measures. The analysis of the recorded subgrade temperature in permafrost regions showed that the east–west and north–south sides of the subgrade have significant ground temperature differences, which can cause an unbalance between the transverse ground temperature field and the artificial permafrost table, further bringing about a transverse deformation difference and inducing longitudinal cracks [10–13]. Through years of real-time data monitoring of the Qinghai–Tibet Railway, Mu et al. [14] found that the differential settlement between the left and right shoulders of some subgrades reached 40 mm after five years, and there was a trend of continuous development. This differential settlement can lead to the generation of longitudinal cracks in the subgrade. An investigation into subgrade cracks in the Qinghai–Tibet Railway showed that the main types of cracks induced were longitudinal ones. Although this problem in HSR subgrades in seasonally frozen regions is not significant owing to ballastless track structure coverage, if it occurs, it would seriously threaten the stability of the ground temperature and deformation of the subgrade.

Currently, the analysis of the transverse ground temperature difference in cold regions is mainly based on field-measured data along with a comparison of the distribution of the temperature difference along the depth at different moments and the changes in the ground temperature over time at different positions. Given the relatively wide spatial and temporal distributions of ground temperature data, the analysis and comparison are mainly qualitative or semi quantitative [5,6,9–13]. Based on the principles of geometry and material science, Liu et al. [15] introduced the concept of thermal static moment to reflect the behaviors of the thermal regime and sunny-shady slope effect in the entire subgrade profile. They found that, the greater the thermal static moment, the greater the asymmetry of the geothermal field. However, the analysis was mainly on the symmetry of the ground temperature distribution at a certain moment; the homogeneity of the ground temperature variation with time at different symmetric locations could not be directly evaluated. For a comprehensive evaluation method, the selection of evaluation indexes should consider not only static indexes that reflect the overall behavior at a certain time, but also dynamic evaluation indexes that reflect the behavior changes in a certain period [16]. Therefore, it is necessary to establish homogeneity and symmetry indices suitable to analyze the spatiotemporal changes in the 2D field and help evaluate the difference in the ground temperature field.

The main objective of ensuring subgrade stability is to evaluate the transverse ground temperature difference and select reasonable mitigation measures. Aiming at the subgrade frost heave problem in seasonally frozen regions, researchers put forward a series of mitigation measures based on engineering practice [3]. These include: (1) replacing the subgrade fillings by coarse-grained soil with a low frost heave ratio [15,17,18] or modified subgrade fillings, such as modified graded crushed stone with cement [19], or modified soil with some modifier [20], and adjusting the composition of each layer [21], which could be used to increase the mechanical performance and thermal resistance of the subgrade; (2) setting a heat preservation berm to improve the thermal resistance of the slope and thereby reducing the quantity of the cold propagating from the slope into the subgrade [22–24]; (3) setting thermal insulation measures to increase subgrade thermal resistance [25–27]; (4) incorporating various thermosyphons to actively input heat to the subgrade [28,29]; (5) setting up or improving drainage measures to reduce water in the subgrade, including preventing water seepage into the subgrade with compound geomembrane or closing all the subgrades, and draining the accumulated water from the fillings via subdrainage holes [30]. The main principle of controlling the frost heave of subgrades in seasonally frozen regions is to reduce the frost depth or control the redistribution and migration of water in the frost depth range. Reducing the frost depth is the most common and

effective measure. The various mitigation measures employed work differently. The thermal insulation properties of the berm, subgrade fillings, and thermal insulation materials are mainly related to its geometry, location in the subgrade, and the thermal conductivity (the lower the thermal conductivity of the materials within the subgrade range, the better the thermal insulation effect). The applicable conditions and effects of each method are different, and the effects of various measures on the prevention and treatment of transverse subgrade deformation differences in seasonally frozen regions have not been studied.

To overcome the research issues addressed, this study: (1) establishs evaluation indices for the transverse ground temperature difference with a clear physical significance applicable to railway subgrades in cold regions, which can be used to evaluate the homogeneity and symmetry in the distribution of the transverse ground temperature field difference; (2) verifies the feasibility and superiority of the proposed transverse ground temperature difference indices by calculating the temperature field and evaluation indices of subgrades with different types of anti-frost heave berms, where a mathematical model which conveniently solve the temperature change will be adopted; (3) calculates the evaluation indices changes in the temperature field of the subgrade after adopting different mitigation measures in seasonally frozen regions to assess its effect in improving the stability of the subgrade ground temperature. This study is of great significance for selecting reasonable mitigation measures in subgrade design and maintenance, providing a theoretical basis and reference for eliminating the transverse ground temperature difference and improving subgrade stability in engineering projects.

2. Proposal and verification of ground temperature difference evaluation indices

2.1. Proposal and calculation of ground temperature difference evaluation indices

In establishing a subgrade evaluation index for railways in cold regions, the range of the subgrade causing frost heave or transverse asymmetric deformation should be mainly considered, with clear physical significance. There are certain internal relationships between the selected indices, which are both independent and correlated. At the same time, the calculation data can be easily obtained, and the selected indices should be obtained through simple operation methods and be easy to implement. The transverse ground temperature difference is mainly displayed within the range of the seasonally frozen layer of the subgrade. The middle line between the two lines, i.e., the central line, is the symmetric line, the ground temperature at the symmetric positions varies with time, and the ground temperatures at the symmetric positions have different variation rules. Therefore, the stability analysis requires both the homogeneity of the ground temperature with time at the line of symmetry and the degree of symmetry of the ground temperature at a certain moment. In other words, this requires the homogeneity in the time domain and symmetry in the spatial domain.

Considering that the ground temperature within the frost depth in a seasonally frozen region contributes the most to soil deformation, the ground temperature data within the frost depth range (the maximum frozen layer depth determined according to the measured data) were selected for the analysis. Based on ground temperature data with a 2D spatial distribution [31,32], this study assumed the transverse lines to be m rows and the longitudinal lines columns to be $2n$; thus, the ground temperature data T form an $m \times 2n$ matrix, defined as two primary target areas with the central line as the dividing line, as shown in Fig. 1. The selection method of the evaluation indices is as follows.

2.1.1. Homogeneity index

The spatial ground temperature data were selected, and the time history of the data in the study area was then treated using the homogeneity coefficient, yielding the time history of the homogeneity coefficient of the ground temperature in the symmetric area; two primary target areas had m rows in the transverse direction and $2n$ in the longitudinal direction. In the primary target point in each group, the ground temperature at time t within the time period h at the ith row and jth column was $T^t_{i,j}$, the ground temperature of the other primary target on the symmetric position at moment t within the time period h at the ith row and $2n$-j+1st column was $T^t_{i,2n-j+1}$, and the homogeneity coefficient of the ground temperature over time in each group was $CU'_{i,j}$. Thus, we have:

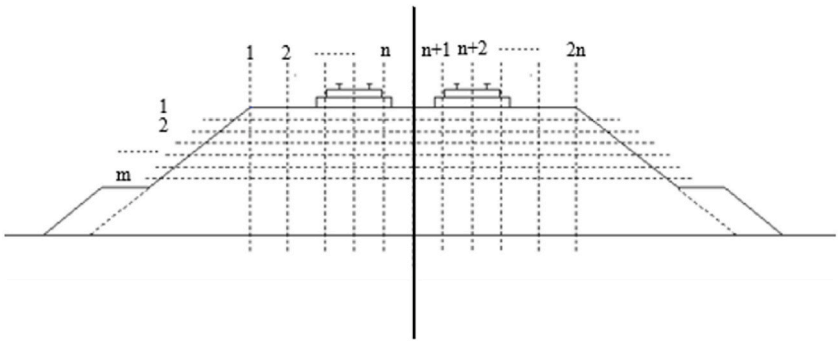

Fig. 1. Division of cross sections of the subgrade.

$$\mathrm{CU}_{i,j}^{'}=\left(1-\sum_{t=1}^{h}\left|\mathrm{T}_{i,j}^{t}-\mathrm{T}_{i,2n-j+1}^{t}\right| \Big/ \sum_{t=1}^{h}\frac{\left|\mathrm{T}_{i,j}^{t}+\mathrm{T}_{i,2n-j+1}^{t}\right|}{2}\right)\times 100\% \tag{1}$$

This equation is inapplicable when $\mathrm{T}_{i,j}^{t}$ is equal to $\mathrm{T}_{i,2n-j+1}^{t}$ and both of them are zero. Nevertheless, this scenario is rare because it is nearly impossible for the two temperatures at symmetric location to be equal and zero simultaneously. The homogeneity coefficients of the ground temperature over the time differences of the symmetric points $\mathrm{CU}_{i,j}^{'}$ were represented in the form of a homogeneity matrix of the ground temperature differences CU.

$$\mathrm{CU}=\begin{bmatrix}\mathrm{CU}_{1,1}^{'} & \mathrm{CU}_{1,2}^{'} & \cdots & \mathrm{CU}_{1,n}^{'}\\ \mathrm{CU}_{2,1}^{'} & \mathrm{CU}_{2,2}^{'} & \cdots & \mathrm{CU}_{2,n}^{'}\\ \cdots & \cdots & \cdots & \cdots\\ \mathrm{CU}_{m,1}^{'} & \mathrm{CU}_{m,2}^{'} & \cdots & \mathrm{CU}_{m,n}^{'}\end{bmatrix} \tag{2}$$

To obtain a comprehensive weighted evaluation index, considering that subgrade surface deformation at the track center is generally the most important factor in subgrade deformation, the influence of ground temperature in each column on the deformation was first studied. The weighting coefficient of the *i*th row and *j*th column in the matrix CU was $\mathrm{f}(i)\times\mathrm{g}(j)$, where $\mathrm{g}(j)$ was no less than 0.5, and $\mathrm{f}(i)$ was also no less than 0.5. Moreover, we have:

$$\sum_{j=1}^{n}\mathrm{g}(j)=1,\sum_{i=1}^{m}\mathrm{f}(i)=1 \tag{3}$$

The evaluation matrix formed by the weight of each element in the matrix CU was denoted by R:

$$\mathrm{R}=\left(\mathrm{r}_{i,j}\right)_{m\times n}=\mathrm{f}(i)\times\mathrm{g}(j) \tag{4}$$

It satisfied

$$\sum_{i=1}^{m}\sum_{j=1}^{n}\mathrm{r}_{i,j}=1 \tag{5}$$

The time history of the homogeneity index of the ground temperature differences in the symmetric zone was denoted by CU^{Z}:

$$\mathrm{CU}^{\mathrm{Z}}=\sum_{i=1}^{m}\sum_{j=1}^{n}\mathrm{CU}_{i,j}^{'}\times\mathrm{r}_{i,j} \tag{6}$$

2.1.2. Symmetry index

The spatial distribution of the ground temperature data was selected to process the symmetry of the ground temperature distribution at different symmetric positions with the same transverse position simultaneously, and the left–right symmetry degree of the data distribution was obtained. The spatial distribution of the ground temperature difference in the target subgrade at a certain moment was judged on the basis of the degree of the left–right symmetry of the ground temperature at this moment.

The evaluation index of the ground temperature symmetry at symmetric positions with different depths in the same horizontal coordinate was represented by the symmetry coefficient of the two columns of the ground temperature at symmetric positions, which could reflect the degree of the left–right symmetry of the data distribution. The symmetry coefficient DC_j can be calculated as follows:

Among the primary target points in each group, the ground temperature of the target point at the *i*th row and *j*th column at a typical time was $\mathrm{T}_{i,j}^{t}$, the ground temperature of the target point at the *i*th row and *2n-j*+1st column at a typical time was $\mathrm{T}_{i,2n-j+1}^{t}$, and the temperature symmetry coefficient is D C_j. Their relationship was expressed as:

$$\mathrm{DC}_j=1-\left(\sum_{i=1}^{m}\frac{\left|\mathrm{T}_{i,j}^{t}-\mathrm{T}_{i,2n-j+1}^{t}\right|}{\max\left(\left|\mathrm{T}_{i,j}^{t}\right|,\left|\mathrm{T}_{i,2n-j+1}^{t}\right|\right)}\right)\Big/ m \tag{7}$$

This equation is inapplicable when $\mathrm{T}_{i,j}^{t}$ is equal to $\mathrm{T}_{i,2n-j+1}^{t}$ and both of them are zero. Nevertheless, this scenario is rare because it is nearly impossible for the two temperatures at a symmetric location to be equal and zero simultaneously, which leads to a $1\times n$ symmetry coefficient matrix DC:

$$\mathrm{DC}=[\mathrm{DC}_1\mathrm{DC}_2\ldots\mathrm{DC}_n] \tag{8}$$

Based on the position of the target points in the ground temperature numerical model, the weight of the ground temperature symmetry coefficient DC_j was determined as $\mathrm{g}(j)$. Let the temperature symmetry index be DC^{Z}.

$$\mathrm{DC}^{\mathrm{Z}}=\sum_{j=1}^{\mathrm{n}}\mathrm{DC}_j\times\mathrm{g}(j) \tag{9}$$

2.2. Calculation of the subgrade temperature difference with different types of anti-frost heave berms and verification of evaluation indices

In this study, DK883 + 330 of the Harbin–Dalian HSR subgrade was chosen as the typical section. The section is located near Shuangcheng Station in Harbin city, with an elevation of 166.4 m. With the north as 0° and Harbin pointing toward Beijing as the direction of the line, the subgrade trend of the section is approximately 210°, slightly deviating from the trend of due south to north, as shown in Fig. 2(a) [9]. Fig. 2(b) shows the section composition, with a height of 5.433 m and a top width of 13.6 m. The frost depth of the natural ground in this region is 1.85 m. The subgrade filling comprises a 0.4 m-thick graded gravel broken stone, insulation layer, and coarse-grained filling. Anti-frost heave berms were set at the foot of the embankment slope, the height and width were set to 2 m, and the slope rate was 1:1.5.

To verify the feasibility and superiority of the ground temperature difference evaluation indices as well as to study the influence of different types of berms on the subgrade temperature field, the changes in the calculated temperature field and the ground temperature difference evaluation indices of three different types of berms were analyzed. The calculation model can be divided into three working conditions based on the heights of the left and right berms: the original 2 m-tall symmetric berms (Figs. 2), 3.7 m-tall symmetric berms (Fig. 3(a)), and 5.433 m-tall asymmetric berms (Fig. 3(b)), with the widths of both the left and right berms being 2 m.

2.2.1. Establishment of numerical model

First, a mathematical model temperature–control equation was proposed based on thermal and mathematical principles. Subsequently, based on the measured data from the monitored section, the initial values and boundary conditions of the numerical simulation were fitted to calculate the thermal parameters of the various materials in the subgrade section. COMSOL Multiphysics was used as the finite element software for the calculations.

(a)

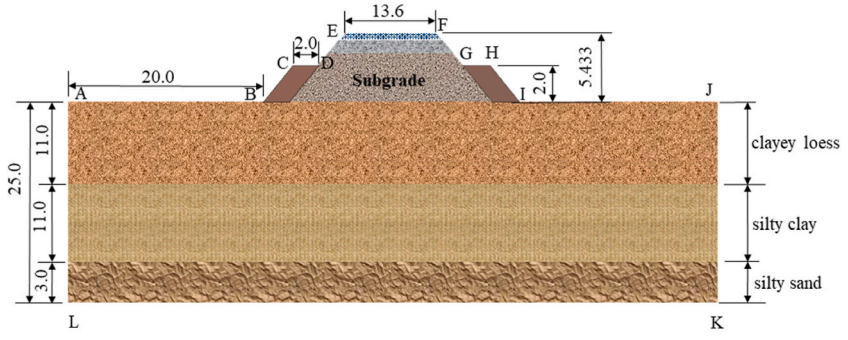

(b)

Fig. 2. Location and geometry of the observation section. (a) Location of the observation section [9]; (b) Cross section of the subgrade (unit: m).

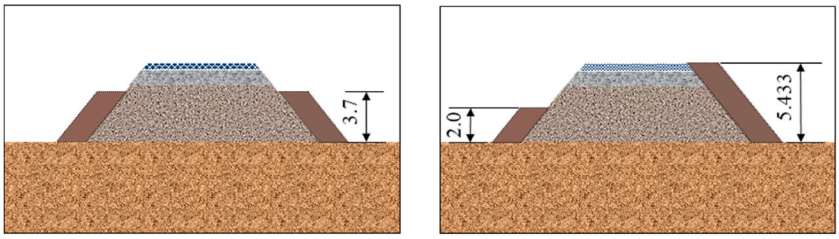

Fig. 3. Other types of berms (unit: m). (a) Symmetric berms with a height of 3.7 m; (b) Asymmetric berms with a maximum height of 5.433 m.

(1) Temperature-control equation

Assuming that the action of the external force of the subgrade soil in the freezing process was not considered, and the heat loss by evaporation, heat convection, and water migration of the subgrade soil were ignored, the differential equation of heat conduction could be established according to the law of energy conservation and Fourier's law as follows [7].

$$T_{i,j}^{t} \tag{10}$$

Given the ice–water phase transition, the temperature at the phase transition interface changed discontinuously with time, whereas the enthalpy changes continuously. Therefore, after introducing the dependent variable enthalpy, the entire object could be directly processed without tracking the two-phase interface. After the enthalpy was introduced, the temperature-control equation could be expressed as equation (11) [7]:

$$T_{i,2n-j+1}^{t} \tag{11}$$

Here, ρ is the density (kg·m^{-3}); c is the specific heat (J·(kg·°C)$^{-1}$); λ is the thermal conductivity (W·(m·K)$^{-1}$); T is the temperature (°C); t is the time (s); H is the enthalpy (J·m^{-3}), which can be obtained as equation (12).

$$T_{i,j}^{t} \ , \ T_{i,2n-j+1}^{t}$$

$$\rho c\frac{\partial T}{\partial t}=\frac{\partial}{\partial x}\left(\lambda\frac{\partial T}{\partial x}\right)+\frac{\partial}{\partial y}\left(\lambda\frac{\partial T}{\partial y}\right) \ , \ \frac{\partial H}{\partial T}\frac{\partial T}{\partial t}=\frac{\partial}{\partial x}\left(\lambda\frac{\partial T}{\partial x}\right)+\frac{\partial}{\partial y}\left(\lambda\frac{\partial T}{\partial y}\right) \tag{12}$$

$$H(T)=\int_{T_r}^{T}\rho c_{df}(T)dT \ , \ T<T_s$$

Here $[H(T) = \int_{T_r}^{T_s}\rho c_{df}(T)dT+\int_{T_s}^{T}\left(\rho\left(\frac{dL}{dT}\right)+\rho c_f(T)\right)dT, T_s \le T \le T_l]$ is the phase-transition temperature, the subscripts l and s indicate the liquid and solid states, respectively, $H(T) = \int_{T_r}^{T_s}\rho c_{df}(T)dT+\rho L+\int_{T_s}^{T_1}\rho c_f(T)dT+\int_{T_1}^{T}\rho c_{du}(T)dT$ and $T > T_1$ are the specific heats of the melted and frozen soils, respectively, T_s is the specific heat during the phase-transition temperature, L is the latent heat, and T_l is the reference temperature, which is lower than T_s.

(2) Determination of the initial and boundary conditions

We conducted field temperature monitoring on the chosen section [33]. The initial temperature at measuring points on August 1, 2010, was adopted as the temperature constraint on the corresponding nodes after the network of the computing model was completed. A steady-state calculation was made, and the calculated result was taken as the initial temperature condition for transient calculation [7].

Fig. 2 presents the calculation model, with the boundary conditions given by equations (13)–(15).

$$T=T(x,y,t),(x,y)\in AB,BC,CD,DE,EF,FG,GH,HI,IJ \tag{13}$$

$$C_{du}(T) \tag{14}$$

$$C_{df}(T) \tag{15}$$

Here, t is the elapsed time (H) from the starting point; T_1 is the temperature of the model at the bottom boundary, which is taken as 7 °C.

The detailed values pertaining to the boundary conditions of the model are as follows [33,34].

(a) Test holes at the toes of the east and west slopes to the natural ground:

Table 1
Thermal and physical parameters of roadbed and foundation soil layers.

Temperature/°C	Graded broken stone			Coarse grained filler			Clayey loess			Silty clay			Silty sand		
	ρ/(kg·m^{-3}	λ (J/(m·h·°C)	H/(10^6 J m^{-3}	ρ/(kg·m^{-3}	λ (J/(m·h·°C)	H/(10^6 J m^{-3}	ρ/(kg·m^{-3}	λ (J/(m·h·°C)	H/(10^6 J m^{-3}	ρ/(kg·m^{-3}	λ (J/(m·h·°C)	C (J/(kg·°C)	ρ/(kg·m^{-3}	λ(J/(m·h·°C))	C(J/(kg·°C)
−10.0	1958	9100.8	0.00	2310	5040	0.00	1700	8640	0.00	2080			1800		
−5.0	1958	9100.8	8.24	2310	5040	8.67	1700	8640	8.84	2080			1800		
−2.0	1958	9100.8	13.22	2310	5040	13.91	1700	8640	11.95	2080			1800		
−1.0	1958	9100.8	14.90	2310	5040	15.68	1700	8640	15.06	2080			1800		
−0.5	1958	9100.8	15.76	2310	5040	16.57	1700	8640	15.85	2080			1800		
0.0	1958	6710.4	16.72	2310	4140	17.57	1700	5544	16.66	2080	5112	1609	1800	3924	1048
30.0	1958	6710.4	81.23	2310	4140	83.62	1700	5544	63.27	2080	5112	1609	1800	3924	1048

$c_f(T)$

T_r where x denotes the distance from the toe.

(b) East toe to the east railway shoulder:

$$\frac{\partial T(x,y)}{\partial n} = 0, (x,y) \in AL, JK;$$

$T(x,y) = T_1, (x,y) \in KL;$ where x denotes the distance from the east toe.

(c) East shoulder to the center line:

$$T(x,y,t) = \left(6.310 - \frac{1.140x}{20}\right) + 29.001 \exp(-0.4657 \times 0.6) \cdot \sin\left(\frac{2\pi t}{8760} + \frac{13\pi}{20} - 0.4657 \times 0.6\right) + \frac{0.04t}{8760}$$

$(x,y) \in AB, IJ;\ x: 0 \rightarrow 20,$ where x denotes the distance from the east shoulder.

(d) Central line to the west shoulder:

$$T(x,y,t) = \left(6.310 - \frac{3.240x}{10.1495}\right) + \left(21.908 - \frac{5.899x}{10.1495}\right) \cdot \sin\left(\frac{2\pi t}{8760} + 0.544\pi - \frac{0.105\pi x}{10.1495}\right) + \frac{0.04t}{8760}$$

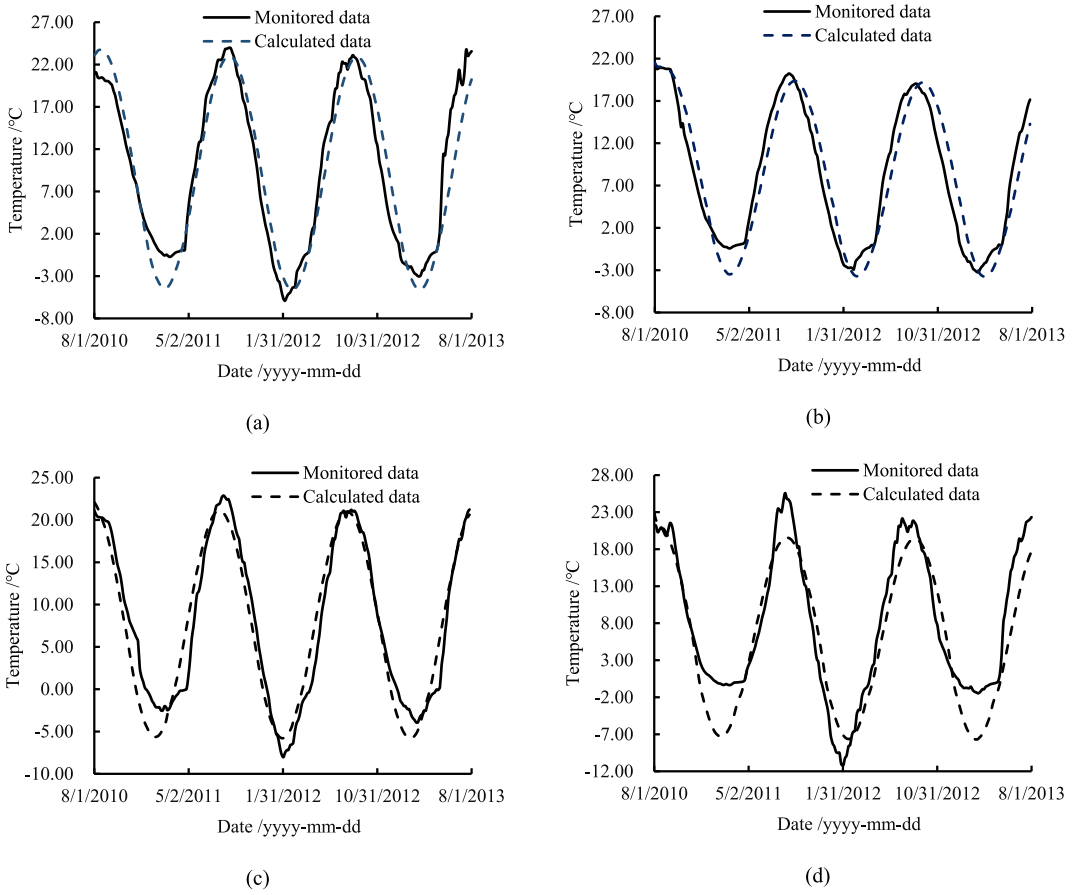

Fig. 4. Comparison between monitored and calculated data at different locations: (a) East shoulder at a depth of 1.3 m; (b) Central line at a depth of 1.3 m; (c) West shoulder at a depth of 1.3 m; (d) Slope toe at a depth of 1.2 m.

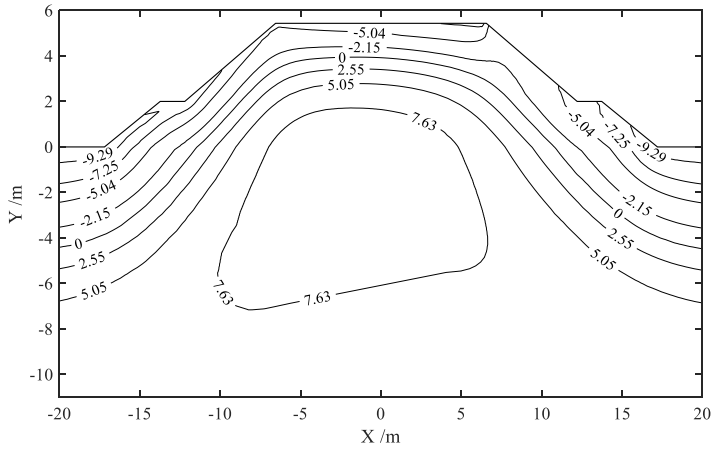

(a)

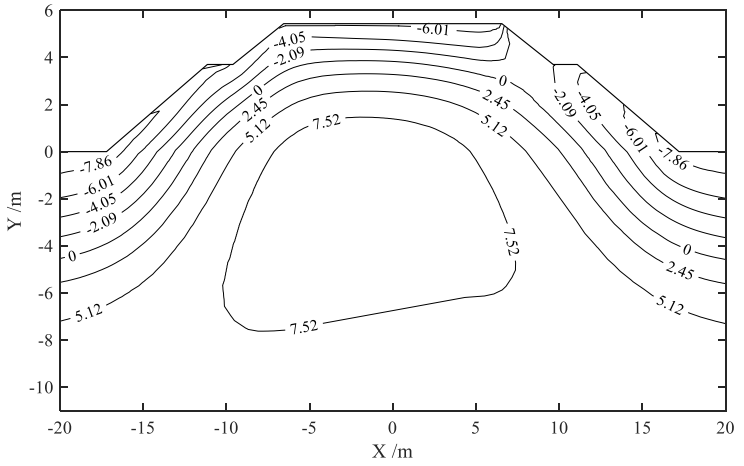

(b)

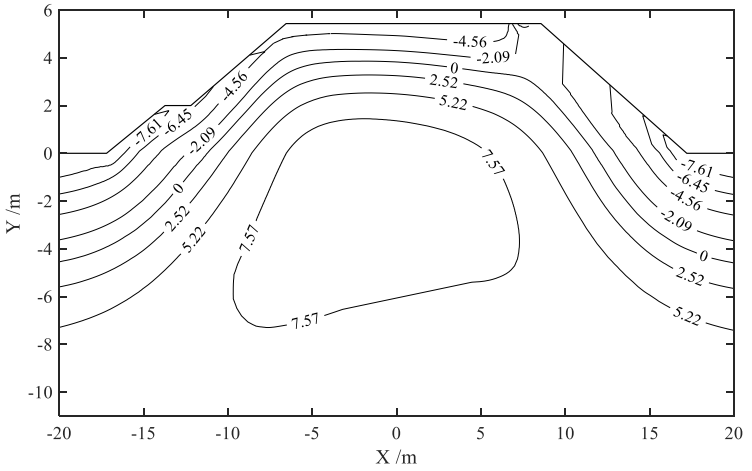

(c)

(caption on next page)

Fig. 5. Nephograms of the temperature distributions of subgrades with different anti-frost heave berms when the maximum frost depth is reached: (a) 2.0 m symmetric berms on 1st March. (Unit: °C); (b) 3.7 m symmetric berms on 3rd March. (Unit: °C); (c) 5.433 m asymmetric berms on 7th March. (Unit: °C).

$$(x, y) \in \mathrm{CD, DE}; x: 0 \rightarrow 10.1495,$$

where x denotes the distance from the east shoulder.

(e) West shoulder to the west toe:

$$\mathrm{T}(x, y, t) = \left(9.550 - \frac{1.843x}{6.8}\right) + \left(18.560 - \frac{1.920x}{6.8}\right)\exp\left(-0.2957 \times 0.5\right) \cdot \sin\left(\frac{2\pi t}{8760} + 0.5\pi - \frac{\pi x}{10 \times 6.8} - 0.2957 \times 0.5\right) + \frac{0.04t}{8760}$$

$x, y \in \mathrm{EF}, x: 0 \rightarrow 6.8,$ where x denotes the distance from the west shoulder.

Here, April 0, 8760 is called the ground temperature growth rate, with the unit of °C/h. The factor 0.04t/8760 was added to each temperature to include the influence of global warming on the ground temperature.

(3) Determination of thermal parameters

Because the selected section is in a seasonally frozen region, the graded broken stone, coarse grained filler layer, and clayey loess layer undergo seasonal freeze–thaw, while silty clay layer and silty sand layer are not frozen all year round. According to the temperature-control equation [34], Eq. (11) is used for materials with phase transition in the process of establishing the calculation model. Inputting the enthalpy H and thermal conductivityλ, Eq. (10) can be used for materials that are always in a single state, and the density, specific heat, and thermal conductivity need to be inputted. Based on the physics of frozen soil [25,26], the parameter values were calculated and listed in Table 1 [7].

2.2.2. Results

The temperature measured at each measurement point on August 1, 2010, was applied to the corresponding nodes behind the network of the calculation model as the temperature constraint, and a steady-state calculation was conducted. The calculation result was used as the initial condition for the transient calculation. The model accuracy was validated by comparing with the monitored data, as shown in Fig. 4 (a) - (d). The model simulation results showed that the subgrade soil starts to undergo unidirectional freezing at the beginning of December each year and reaches its maximum frost depth in mid-March of the next year, and the two-way melting from early April to mid-late April is consistent with the measured results [34].

The nephograms of the temperature distribution when the subgrade reached the maximum frost depth under different working conditions were selected for the analysis (Fig. 5(a)-(c)). Here, X is the distance from the subgrade center, and Y is the subgrade height. As shown in Fig. 5(a)–(c), the ground temperature field distribution within the subgrade range was affected to some extent by the anti-frost heave berms, and the ground temperature at the upper part of the subgrade was slightly increased.

Fig. 6 shows the curves of the maximum frost depths in subgrades with different anti-frost heave berms. Here, X is the distance from the subgrade center, and Y is the subgrade height. As observed, in terms of reducing the frost depth, the maximum frost depth line of the soil on the east and west sides of the subgrade increases gradually with the berm height, indicating that the anti-frost heave berms of the two new types of subgrades were better than that of the existing symmetric subgrade with a height of 2.0 m. Based on the

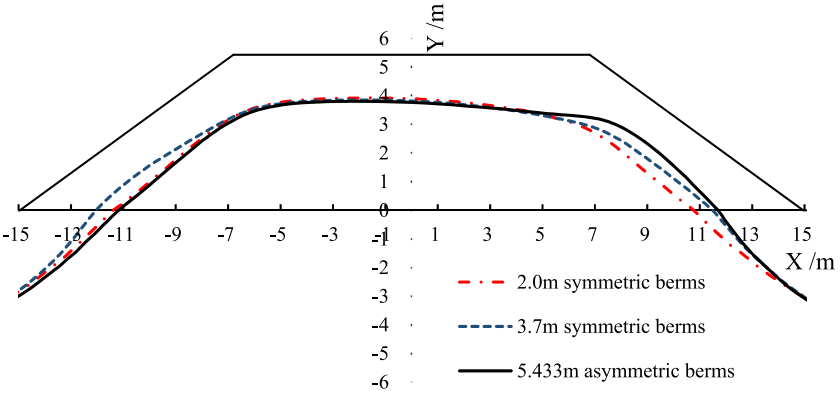

Fig. 6. Curves of the maximum frost depths in subgrades with different anti-frost heave berms (Unit: m).

analysis of the reduction degree of the transverse ground temperature difference of the subgrade, the maximum frost depths on the left and right sides of the subgrade were found to be different, and the left side was smaller than the right side, indicating that only the right-side berm height increases, i.e., the nonsymmetry type might be superior to the 3.7 m symmetric type.

2.3. Index calculation

Combined with on-site ground temperature and deformation monitoring data, soil frost heave was found to contribute the most in the range of 1.0–1.2 m; therefore, the monitored section mainly comprised vertical control lines, such as the left and right shoulders and the center of the left and right tracks, as shown in Fig. 2. Vertically, the center of the line was taken as the central line. As for the distance between them, some other factors were considered. First, half of the subgrade surface width was set to 6.8 m; second, the distance between centers of the tracks was set to 5.0 m, which means the distance from the center of the tracks to the central line was 2.5 m; third, the subgrade part around the center of both tracks was the main concerned range as it mostly influences the subgrade deformation and track performance. Based on these factors and to make the calculation process easy and practical, the distances between the vertical control lines were set to 0, 1.5, 1.5, 1.3, 1.25, and 1.25 m, from the railway shoulder to the central line. The subgrade depths were set to 0, 0.5, 0.8, 1.2, 2.0, and 3.0 m, and taken as the horizontal control lines along the depth direction. The ground temperature at the intersection point was taken as the research object, and T was expressed in the form of a 6 × 5 matrix. Based on the contribution and distribution of the temperature differences, considering that the temperature difference was more evident at shallower depths and that the freezing front significantly influences the temperature field, the weights of the homogeneity for each row from top to bottom were set to 0.05, 0.15, 0.15, 0.20, 0.20, and 0.25. For the columns, because the temperature differences gradually decreased from the shoulder to the central line, the weights were taken as 0.6, 0.15, 0.15, 0.05, and 0.05. According to Eq. (4), the evaluation matrix R was obtained.

$$\mathrm{R}=\begin{bmatrix}0.03 & 0.0075 & 0.0075 & 0.0025 & 0.0025\\ 0.09 & 0.0225 & 0.0225 & 0.0075 & 0.0075\\ 0.09 & 0.0225 & 0.0225 & 0.0075 & 0.0075\\ 0.12 & 0.03 & 0.03 & 0.01 & 0.01\\ 0.12 & 0.03 & 0.03 & 0.01 & 0.01\\ 0.15 & 0.0375 & 0.0375 & 0.0125 & 0.0125\end{bmatrix}$$

Downward from the subgrade surface

$$CU^{'Z}=\sum_{i-1}^{m}\sum_{j-1}^{n}CU^{'}\times r_{i,j}=0.3284$$

According to Eqs. (1)–(6), this study calculated the

$$\mathrm{T}(x,y,t)=\left(7.707+\frac{0.081(x-6.8)}{6.8}\right)+\left(16.640+\frac{2.700(x-6.8)}{6.8}\right)\exp\left(-0.2957\times 0.5\right)\cdot\sin\left(\frac{2\pi t}{8760}+0.4\pi+\frac{\pi(x-6.8)}{10\times 6.8}-0.2957\times 0.5\right)+\frac{0.04t}{8760}$$

and CU^{Z} values of subgrades with different anti-frost heave berms. The time was taken as the period from the beginning of freezing (November 24) to the time when the maximum frost depth (March 5) was reached after the temperature field was steady.

The homogeneity index of the subgrade with 2 m symmetric berms was as follows.

$$\mathrm{CU}^{'}=\begin{bmatrix}28.21\% & 61.22\% & 71.60\% & 81.11\% & 90.52\%\\ 3.75\% & 51.03\% & 67.95\% & 80.08\% & 90.45\%\\ -13.76\% & 43.65\% & 66.89\% & 80.72\% & 91.09\%\\ -27.69\% & 42.11\% & 69.97\% & 84.06\% & 92.70\%\\ -1.76\% & 59.75\% & 81.54\% & 90.60\% & 95.90\%\\ 49.91\% & 76.02\% & 88.25\% & 94.01\% & 97.41\%\end{bmatrix}$$

Downward from the subgrade surface

From the shoulder to the central line

$$CU^{'Z}=\sum_{i-1}^{m}\sum_{j-1}^{n}CU^{'}\times r_{i,j}=0.3537$$

$$(x,y)\in \mathrm{EF}, x: 6.8\rightarrow 13.6,$$

The homogeneity index of the subgrade with 3.7 m berms was as follows.

$$\mathrm{CU}' = \begin{bmatrix} 30.62\% & 61.86\% & 72.15\% & 81.50\% & 90.72\% \\ 6.84\% & 52.46\% & 68.56\% & 80.36\% & 90.49\% \\ -8.54\% & 45.20\% & 67.08\% & 80.64\% & 91.91\% \\ -21.08\% & 42.71\% & 69.44\% & 83.46\% & 92.41\% \\ 1.65\% & 59.03\% & 80.65\% & 90.00\% & 95.62\% \\ 53.11\% & 76.31\% & 88.01\% & 93.78\% & 97.28\% \end{bmatrix}$$

$$\mathrm{T}(x,y,t) = \left(7.788 - \frac{1.478x}{10.1495}\right) + \left(16.682 - \frac{5.226x}{10.1495}\right) \cdot \sin\left(\frac{2\pi t}{8760} + 0.659\pi - \frac{0.105\pi x}{10.1495}\right) + \frac{0.04t}{8760}$$

The homogeneity index of the subgrade with 5.433 m asymmetric berms was as follows:

$$(x,y) \in \mathrm{FG, GH}, x: 0 \rightarrow 10.1495,$$

$$\mathrm{CU}^{'}$$

Due to the existence of positive and negative temperatures, the calculated coefficient could be negative; therefore, some of the calculation results of the middle part did not have a significant reference value. The following could be concluded from the above three matrices.

(1) Based on the data of the 2 m-high symmetric berms, the homogeneity coefficient under the east–west shoulder was relatively low, and there was a significant temperature difference, due to the effect of a sunny-shady slope, which is prone to induce asymmetric deformation. The homogeneity coefficient from the shoulder to the central line increased gradually, indicating a gradual decrease in the temperature difference from the shoulder to the central line.
(2) Based on the entire data, the homogeneity coefficient at the same location increased with increasing depth, and the deeper the subgrade, the better homogeneity, the lower the temperature difference, the greater the stability of the subgrade, and the more unlikely the occurrence of a nonuniform deformation.
(3) A comparison of the homogeneity coefficients of the three types of subgrades showed that the temperature field at the center of the embankment was significantly affected by the change in the berm height. The homogeneity coefficient variations over the elapsed time of the ground temperature in the symmetric region obtained from the 3.7 m symmetric berms were relatively small compared with that of the original subgrade. In comparison, the homogeneity coefficient variations in the ground temperature over time in the symmetric region obtained from the 5.433 m asymmetric berms were more significant, greater than those of the other two types, indicating that the difference in the ground temperature in the 5.433 m asymmetric berms changed relatively evenly over time.

According to Eqs. (7)–(9), the DC' and DC^{Z} values of the subgrades with different berms were calculated. The matrix for the ground temperature symmetry indices at a typical moment, i.e., the moment (March 5) when the maximum frost depth was reached in the 2 m symmetric berms, was:

$$CU^{'Z} = \sum_{i=1}^{m} \sum_{j=1}^{n} CU^{'} \times r_{i,j} = 0.5272$$

$$\mathrm{CU}^{'} = \begin{bmatrix} 37.66\% & 68.09\% & 73.49\% & 81.43\% & 90.49\% \\ 35.17\% & 53.06\% & 68.83\% & 80.10\% & 90.36\% \\ 33.15\% & 46.98\% & 67.368\% & 80.83\% & 91.14\% \\ 5.39\% & 43.03\% & 70.83\% & 83.90\% & 92.82\% \\ 48.13\% & 62.12\% & 82.22\% & 90.72\% & 95.94\% \\ 69.43\% & 78.13\% & 88.91\% & 94.17\% & 97.44\% \end{bmatrix}$$

The matrix for the ground temperature symmetry indices at a typical moment, i.e., the moment (March 3) when the maximum frost depth was reached in the 3.7 m symmetric berms, was:

The matrix for the ground temperature symmetry indices at a typical moment, i.e., the moment (March 3) when the maximum frost depth was reached in the 5.433 m asymmetric berms, was.

$$\mathrm{DC}^{'} = \underbrace{\begin{bmatrix} 42.13\% & 52.51\% & 53.03\% & 65.32\% & 93.81\% \end{bmatrix}}_{\text{From the shoulder to the central line}}$$

$$\mathrm{g}(j) = \begin{bmatrix} 0.6 & 0.15 & 0.15 & 0.05 & 0.05 \end{bmatrix}$$

$$DC^Z = \sum_{j-1}^{n} DC_j \times g(j)$$

It is concluded from the matrices that:

The closer the ground temperature to the central line, the higher the left-right symmetry degree, indicating that the degree of symmetry was mainly related to the influence of the east and west symmetric positions. The higher the subgrade berm, the more balanced the spatial distribution of the ground temperature data; thus, the higher the left–right symmetry degree of the data distribution. Asymmetric berms were better than symmetric berms.

From the calculation results, the homogeneity index over time of the ground temperature and typical ground temperature symmetry index of the subgrade with 5.433 m asymmetric berms are greater than those of the other two types of subgrades; the frost depth of the subgrade with 5.433 m asymmetric berms was lower than that of the other two types of subgrades. The changes obtained from the conventional analysis and the evaluation indices proposed in this study were consistent, confirming the feasibility of the calculation method of the evaluation index of the ground temperature difference proposed in this study. In addition, compared with the conventional semi quantitative method employed for the ground temperature, the establishment of the evaluation indices can help evaluate the temporal and spatial changes in the ground temperature and provide suggestions for corresponding mitigation measures. Based on the calculation results, it is suggested to raise the height of the berms in the shady slope in practical projects if measures of adjusting anti-frost heave berms are adopted.

3. Comparison and optimization of mitigation measures based on the evaluation indices of the ground temperature difference

3.1. Mitigation measures

In addition to anti-frost heave berms, thermal insulation materials are common mitigation measures for subgrades in seasonally frozen regions. According to the *Code for Design for Application of Geosynthetics on Subgrade of Railway* (TB 10118-2006) [35], expanded polystyrene (EPS) is a lightweight geomaterial prepared by molding or extrusion when polystyrene is added with a foaming agent. EPS

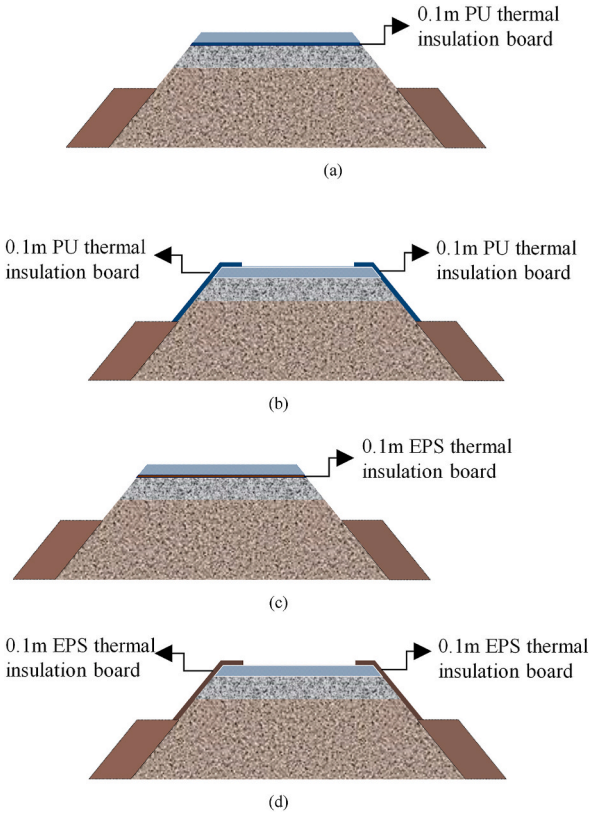

Fig. 7. Four working conditions for placing thermal insulation materials: (a) PU thermal insulation board placed on the surface of the subgrade bed bottom layer–working condition 1; (b) PU thermal insulation board placed on both sides of the slope above the railway shoulder and the berm–working condition 2; (c) EPS thermal insulation board placed on the surface of the subgrade bed bottom layer–working condition 3; (d) EPS thermal insulation board placed on both sides of the slope above the railway shoulder and the berm–working condition 4.

or a polyurethane (PU) insulation board can be laid in frozen regions. In numerical simulations, different types of thermal insulation materials were adopted to study the influence of thermal insulation materials on the subgrade temperature field under different working conditions. Two commonly used insulating boards, namely EPS and PU thermal insulation boards, were selected as the thermal insulation materials, respectively.

When a newly built railway subgrade top layer needs to be treated, geosynthetic materials should be laid on the surface of the subgrade bed bottom layer. Accordingly, thermal insulation materials were laid on the surface of the subgrade bed bottom layer in this study. Different from the newly built subgrade, considering that the existing HSR subgrade has a ballastless track board, with regard to the freezing damage remediation for the existing HSR subgrade, the thermal insulating materials can only be laid outside the track bed and on both sides of the subgrade slope. Meanwhile, to protect the thermal insulating materials, fiber concrete was poured on top of them.

In this study, the typical subgrade section DK883 + 330 of the Harbin–Dalian Railway was also taken as the study object, and four working conditions were set (see Fig. 7(a)–(d)): a PU thermal insulation board was placed on the surface of the subgrade bed bottom layer (working condition 1), PU insulation boards were placed on both sides of the slope above the railway shoulder and the berm (working condition 2), an EPS insulation board was placed on the subgrade bed bottom layer (working condition 3), and an EPS insulation board was placed on both sides of the slope above the railway shoulder and the berm (working condition 4).

3.2. Parameters for calculation

Thermal insulation materials are used in practical engineering to achieve thermal insulation effect. The thermal conductivity is related to the material structure and density. Table 2 presents the thermal and physical parameters of the thermal insulation materials studied [22,23].

3.3. Results and discussions of evaluation index of ground temperature difference

As shown in Fig. 8(a)-(d), the nephograms of the temperature distribution under the four working conditions on 5th March were selected for the analysis. Here, X is the distance from the subgrade center, and Y is the subgrade height. The ground temperature field distribution within the subgrade range was evidently affected by the insulation material placement and its positions, particularly under working conditions 1 and 3 when the insulation board was placed on the surface of the subgrade bed bottom layer.

The evaluation indices of the ground temperature difference of three types of anti-frost heave berms and four types of thermal insulation materials were compared and shown in Table 3. The mitigation rate in this table was defined as the specific value between the indices difference and the indices of the original section. The indices difference was the difference value between the sections with adopted measures and the original section.

Based on the results of the evaluation indices and the mitigation rate of the thermal insulation materials under the four working conditions, working condition 1 with the insulation materials was found to yield a homogeneity index of 0.6498 and a homogeneity mitigation rate of 97.87%, which was higher than those obtained under the other three conditions and all the sections with different anti-frost berms. The calculated results under the four working conditions where thermal insulation materials were used in the subgrades show that the overall symmetry coefficients obtained by laying a PU thermal insulation board on the surface of the subgrade bed bottom layer was higher than those obtained under the other three working conditions. This indicated that the ground temperature of the PU thermal insulation board had the highest degree of left–right symmetry, and the spatial distribution of the ground temperature difference of the target subgrade at this time was relatively balanced.

In Table 3, the homogeneity mitigation rates of the sections with different anti-frost berms were 7.70% and 60.54%, and the symmetry mitigation rates were 5.13% and 37.48%. The homogeneity mitigation rates of the sections with different thermal insulation ranged from 28.05% to 97.87%, and the symmetry mitigation rates ranged from 32.17% to 45.90%. Compared with anti-frost heave berms, although both the berms and thermal insulation materials reduced the amount of cold entering the subgrade from outside, thermal insulation materials had a more significant effect in eliminating the ground temperature difference. This study recommends placing thermal insulation boards on the surface of the subgrade bed bottom layer in practical engineering. The frost depth and ground temperature difference can be effectively reduced to ensure the safe operation of railways.

The evaluation indices of the ground temperature difference proposed in this study can be based on a qualitative comparison of the spatiotemporal distribution of the ground temperature field in cold regions. The homogeneity and symmetry of the subgrade ground temperature field can be comprehensively compared in a quantitative manner. This is not only conducive to analyze the distribution characteristics of the subgrade ground temperature field, but more importantly, it can be used as a basis to quantitatively compare the advantages and disadvantages of various mitigation measures and further optimize the selected mitigation measures accordingly. Through the calculation and analysis in this study, from the perspective of eliminating ground temperature difference, if a subgrade is already in operation, the ground temperature difference can be reduced by increasing the height of the anti-frost heave berms on the

Table 2
Thermal and physical parameters of thermal insulation materials.

Thermal insulation materials	ρ (kg·m^{-3})	λ (W/(m·°C))	C (J/(kg·°C)
EPS	40	0.0350	1400
PU	57	0.0197	2475

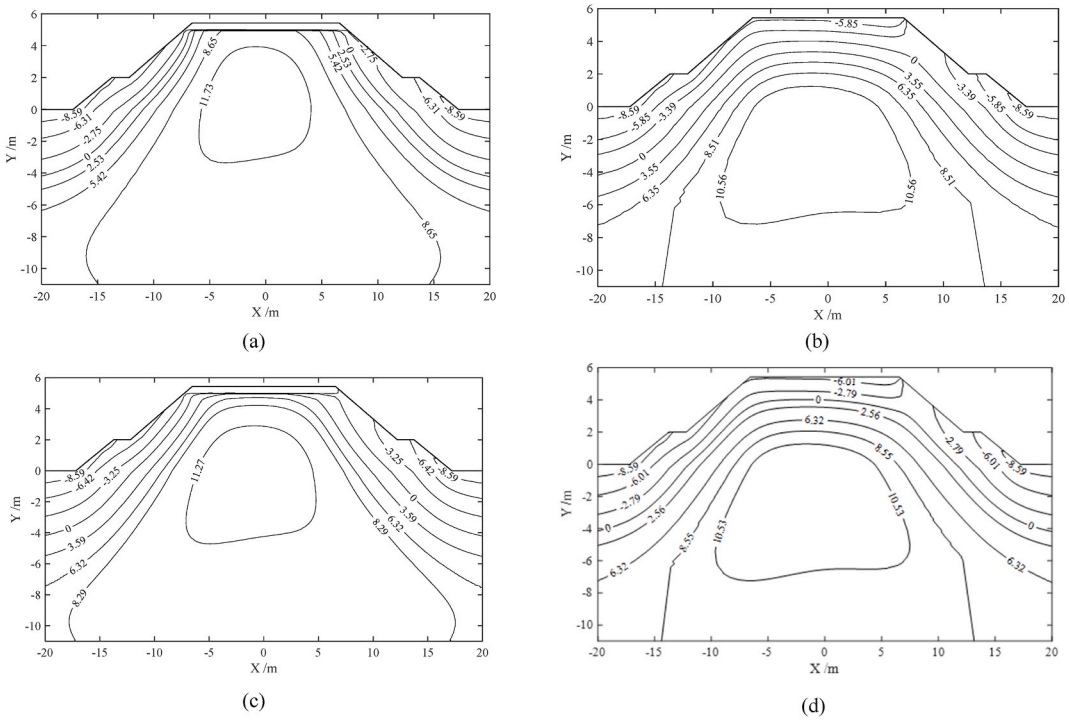

Fig. 8. Nephograms of the temperature distributions of subgrades with thermal insulation materials when the maximum frost depth is reached. (a) PU thermal insulation board placed on the surface of the subgrade bed bottom layer–working condition 1; (b) PU thermal insulation board placed on both sides of the slope above the railway shoulder and the berm–working condition 2; (c) EPS thermal insulation board placed on the surface of the subgrade bed bottom layer–working condition 3; (d) EPS thermal insulation board placed on both sides of the slope above the railway shoulder and the berm–working condition 4.

Table 3
Evaluation indices for the ground temperature difference.

Mitigation measure	Homogeneity index	Symmetry index	Mitigation rate: Homogeneity	Mitigation rate: Symmetry
2.0 m original berms	0.3284	0.4856		
3.7 m symmetric berms	0.3537	0.5105	7.70%	5.13%
5.433 m asymmetric berms	0.5272	0.6676	60.54%	37.48%
thermal insulation materials–working condition 1	0.6498	0.7085	97.87%	45.90%
thermal insulation materials–working condition 2	0.4504	0.6568	37.15%	35.26%
thermal insulation materials–working condition 3	0.5143	0.6665	56.61%	37.25%
thermal insulation materials–working condition 4	0.4205	0.6418	28.05%	32.17%

shady slope side, thus enhancing the subgrade stability.

4. Conclusions

An efficient and comprehensive method to evaluate the transverse temperature difference of a subgrade was developed in this study. This method is aimed to compare the time history of the homogeneity and symmetry indices of the ground temperature at typical moments by putting forward homogeneity and symmetry indices. Based on this method, the indices were used to compare the efficiency of embankments with several mitigation measures, which could be used to reduce or eliminate the transverse temperature difference. The conclusions of the study are as follows.

(1) The method could be used to evaluate the change in the subgrade ground temperature difference over time and the spatial distribution characteristics of this difference at a certain moment.
(2) The frost depth of the subgrade could be effectively reduced by increasing the height of the anti-frost heave berms. The homogeneity and symmetry indices of the asymmetric anti-frost berms were higher than those of the symmetric berms. The homogeneity mitigation rates ranged from 7.70% to 60.54%, and the symmetry mitigation rates ranged from 5.13% to 37.48%, indicating a relatively balanced temperature distribution of the subgrade with asymmetric berms.

(3) Once the thermal insulation materials were placed, the homogeneity and symmetry indices of the PU thermal insulation board were superior to those of the EPS thermal insulation board. Placing the thermal insulation board on the surface of the subgrade bed bottom layer had a better effect than placing it on the shoulder and on both sides of the slope above the berms. The homogeneity mitigation rates ranged from 28.05% to 97.87% and the symmetry mitigation rates ranged from 32.17% to 45.90%. The homogeneity and symmetry of the subgrade ground temperature were superior to those of the subgrade with anti-frost berms after placing the thermal insulation materials.

Based on the proposed evaluation index system for the ground temperature in this study, subsequent mitigation measures can be optimized from various aspects. In addition, the process of the evaluation index calculation before the field monitoring can provide reference for the monitoring point arrangement and data analysis; for example, how to consider the distance between the control lines and weights of each temperature point can be used to determine the locations of the temperature sensor chains that are embedded during subgrade construction; the matrices of the homogeneity and symmetry, $DC^Z = \sum_{j=1}^{n} DC_j \times g(j)$ and $DC^Z = 0.4856$, can help locate the potential maximum temperature difference or deformation difference. However, this study mainly investigated the 2D temperature field distribution at the cross section of a subgrade. In practical engineering, a subgrade takes a 3D shape. Hence, the homogeneity and symmetry indices of the ground temperature in a 3D space should be investigated to explore mitigation measures that can improve the evaluation indices of the ground temperature difference and subgrade stability in the 3D space.

Author contribution statement

Yu-zhi Zhang: Conceived and designed the experiments; Contributed reagents, materials, analysis tools or data; Wrote the paper.
Xiao-jie Liang: Performed the experiments; Analyzed and interpreted the data.
Ya-qian Dong, Zhi-rong Zhao: Analyzed and interpreted the data; Wrote the paper.
Cheng-yan Li: Analyzed and interpreted the data; Contributed reagents, materials, analysis tools or data.

Data availability statement

Data will be made available on request.

Declaration of competing interest

The authors declare that they have no known competing financial interests or personal relationships that could have appeared to influence the work reported in this paper.

Acknowledgments

This research was funded by the National Natural Science Foundation of China (NSFC) under grant nos. 52078312; Key Research and Development Plan Project of Hebei Province under grant no.19210804D; Science and Technology Development Foundation of Colleges and Universities in Hebei Province under grant no. ZD2020335; CCCC Science and Technology R&D Project under grant no. 2021-ZJKJ-01; Technology development project of Shuohuang Railway Development Co., Ltd. under grant no. GJNY-20-230 and Innovative Research Group Project of Natural Science Foundation of Hebei Province under grant no. E2021210099. The authors would also like to thank all the reviewers who participated in the review process and MJEditor (www.mjeditor.com) for its linguistic assistance during the preparation of this manuscript.

References

[1] F.J. Niu, H. Liu, Y.H. Niu, Experimental study of freeze characteristics in roadbed-culvert transition section along a high-speed railway, Chin. J. Rock Mech. Eng. 33 (2014) 639–646. https://doi:10.13722/j.cnki.jrme.2014.03.024.
[2] F.J. Niu, A.Y. Li, J. Luo, Z.J. Lin, G.A. Yin, M.H. Liu, H. Zheng, H. Liu, Soil moisture, ground temperatures, and deformation of a high-speed railway embankment in Northeast China, Cold Reg. Sci. Technol. 133 (2017) 7–14, https://doi.org/10.1016/j.coldregions.2016.10.007.
[3] F.J. Niu, H. Zheng, A.Y. Li, The study of frost heave mechanism of high-speed railway foundation by field-monitored data and indoor verification experiment, Acta Geotech. 15 (2020) 581–593, https://doi.org/10.1007/s11440-018-0740-8.
[4] Q. Miao, F.J. Niu, Z.J. Lin, J. Luo, M.H. Liu, Comparing frost heave characteristics in cut and embankment sections along a high-speed railway in seasonally frozen ground of Northeast China, Cold Reg. Sci. Technol. 170 (2019), 102921, https://doi.org/10.1016/j.coldregions.2019.102921.
[5] B.W. Tai, Z.R. Yue, J.K. Liu, Y.P. Shen, Y.H. Tian, J.H. Fang, Analysis on difference of ground temperature and deformation between southern and northern sides of high-speed railway embankment in cold regions, J. China Railw. Soc. 39 (3) (2017) 82–89. https://doi:10.3969/j.issn.1001-8360.2017.03.014.
[6] Y.Z. Zhang, B.C. Sun, P. Li, X.J. Liang, J. Yang, Analysis of deformation and temperature characteristics of high-speed railway roadbed in seasonal frozen regions, Soil Mech. Found. Eng. 57 (5) (2020) 384–393. https://doi:10.1007/s11204-020-09682-z.
[7] Y.Z. Zhang, Y.L. Du, B.C. Sun, Temperature distribution in roadbed of high-speed railway in seasonally frozen regions, Chin. J. Rock Mech. Eng. 33 (6) (2014) 1286–1296. https://doi:10.13722/j.cnki.jrme.2014.06.023.
[8] Y.Z. Zhang, Y.L. Du, B.C. Sun, S.P. Zhang, J. Han, Roadbed deformation of high-speed railway due to freezing-thawing process in seasonally frozen regions, Chin. J. Rock Mech. Eng. 33 (12) (2014) 2546–2553. https://doi:10.13722/j.cnki.jrme.2014.12.021.
[9] Y.Z. Zhang, B.C. Sun, A. Wen, Cheng BY, Transverse thermal regime difference of high-speed railway roadbed in seasonally frozen regions, Proc. Instit Civil Eng. Ground Improv. 172 (4) (2019) 264–273. https://doi:10.1680/jgrim.18.00040.
[10] Y.L. Chou, Y. Sheng, Y.W. Li, Z.M. Wei, Y.P. Zhu, J.P. Li, Sunny-shady slope effect on the thermal and deformation stability of the highway embankment in warm permafrost regions, Cold Reg. Sci. Technol. 63 (2010) 78–86, https://doi.org/10.1016/j.coldregions.2010.05.001.

[11] Q.H. Yu, K. Fan, Y.H. You, Y. Guo, L. Yuan, Comparative analysis of temperature variation characteristics of permafrost roadbeds with different widths, Cold Reg. Sci. Technol. 117 (2015) 12–18, https://doi.org/10.1016/j.coldregions.2015.05.002.
[12] Q.B. Wu, Y.Z. Liu, Z.Y. Hu, The thermal effect of differential solar exposure on embankments along the Qinghai–Tibet railway, Cold Reg. Sci. Technol. 66 (2011) 30–38, https://doi.org/10.1016/j.coldregions.2011.01.001.
[13] Y.L. Chou, Y. Sheng, J. Chen, X. Chen, Analysis on thermal stability and deformation stability of CMR, Cold Reg. Sci. Technol. 110 (2015) 215–222, https://doi.org/10.1016/j.coldregions.2014.10.004.
[14] Y.H. Mu, W. Ma, F.J. Niu, G. Liu, Q.L. Zhang, Study on geotechnical hazards to roadway engineering in permafrost regions, J. Disas. Preven. Mitig. Eng. 34 (2014) 259–267. https://doi:10.13409/j.cnki.jdpme.2014.03.005.
[15] H. Liu, F.J. Niu, H. Guan, An engineering evaluation index of thermal asymmetry in subgrade and its optimal design in cold regions, Cold Reg. Sci. Technol. 137 (2017) 1–6, https://doi.org/10.1016/j.coldregions.2017.02.001.
[16] X. Fu, G. Zhao, M.M. Wang, J. Wang, Y. Xu, C.S. Gu, Comprehensive evaluation method for structural behavior of concrete dams in cold regions, Eng. Struct. 278 (2023), 115435, https://doi.org/10.1016/j.engstruct.2022.115435.
[17] H. Liu, F.J. Niu, Y.H. Niu, Z.J. Lin, J.H. Luo, Study of design of filling material and setting anti-frost layer for high-speed railway roadbed in seasonally frozen regions, Chin. J. Rock Mech. Eng. 30 (12) (2011) 2549–2557. https://doi:10.3969/j.issn.1001-8360.2011.03.015.
[18] Z.R. Yue, T.L. Wang, C. Ma, et al., Frost heave control of fine round gravel fillings in deep seasonal frozen regions, Sci. Cold Arid Regions 5 (4) (2013) 425–432.
[19] S.J. Tian, Experimental study on frost heaving characteristics of graded cobble mixed with cement for Harbin-Dalian High Speed Railway subgrade, Railw. Eng. 8 (2014) 79–82.
[20] Z.W. Xiong, L. Jin, J. Cheng, et al., Experimental study on frost heaving characteristics of improved coarse grain filling for high speed railway, China Railw. Sci. 36 (5) (2015) 1–6.
[21] B.W. Tai, Z.R. Yue, T.C. Sun, , Q SC, L. Li, Z.H. Yang, Novel anti-frost subgrade bed structures a high-speed railway in deep seasonally frozen ground regions: Experimental and numerical studies, Constr. Build. Mater 269 (2021), 121266, https://doi.org/10.1016/j.conbuildmat.2020.121266.
[22] J. Xu, F.J. Niu, Y.H. Niu, Z.J. Lin, Z.Y. Xu, Study on the temperature field of insulated roadbed with frost-resistant berm on seasonal frozen region, J. China Railw. Soc. 33 (3) (2011) 84–90. https://doi:10.3969/j.issn.1001-8360.2011.03.015.
[23] X.Y. Xu, H. Qin, Y.S. Ma, Numerical simulation for the temperature field of embankment using thermal-insulation treatment, Cryog. Constr. Techn. 155 (2011) 98–100. https://doi:CNKI:SUN:DRAW.0.2011-05-046.
[24] A. Wen, Y.Z. Zhang, W.G. Zhao, Influence analysis on the water freezing characteristic caused by frost-resistant berm type of high-speed railway subgrade in seasonal frozen region, J. Shijiaz. Tiedao Univer. (Natural Science Edition) 32 (3) (2019) 27–33. https://doi:10.13319/j.cnki.sjztddxxbzrb.20180037.
[25] J. Xu, F.J. Niu, A.M. Li, Z.J. Lin, Analysis of the prevention effect of thermal-insulation method on frost heave of railway subgrade in seasonal frozen regions, J. China Railw. Soc. 32 (6) (2010) 124–131. https://doi:10.3969/j.issn.1001-8360.2010.06.021.
[26] X.Z. Xu, J.C. Wang, L.X. Zhang, Physics of Frozen Soils, Science Press, Beijing, 2010, pp. 40–120 (in Chinese).
[27] Y. Hu, Research on Application of EPS Thermal Insulation Material for Perennial Permafrost Roadbed Project in Qinghai-Tibet Plateau, Dissertation, Southwest Jiaotong University, 2003.
[28] J.Q. Gao, Y.M. Lai, M.Y. Zhang, D. Chang, The thermal effect of heating two-phase closed thermosyphons on the high-speed railway embankment in seasonally frozen regions, Appl. Therm. Eng. 141 (2018) 948–957, https://doi.org/10.1016/j.applthermaleng.2018.06061.
[29] T.F. Hu, J.K. Liu, Z.R. Yue, L. Bao, K.K. Yu, J.Y. Zhang, Study on solar active heating device for subgrade in seasonally frozen soil region, China Railw. Sci. 42 (2) (2021) 39–49. https://doi:10. 3969/j. issn.1001- 4632.2021.02.05.
[30] F.J. Niu, H. Hu, M.H. Liu, et al., Studies for frost heave characteristics and the prevention of the high-speed railway roadbed in the Zoige Wetland, China, Front. Earth Sci. 9 (2021), 678655.
[31] S. Tian, M. Barigou, An improved vibration technique for enhancing temperature uniformity and heat transfer in viscous fluid flow, Chem. Eng. Sci. 123 (2010) 609–619. https://doi:10.1016/j.ces.2014.11.029.
[32] J.M. Jackson, M.L. Hupert, S.A. Soper, Discrete geometry optimization for reducing flow non-uniformity, asymmetry, and parasitic minor loss pressure drops in Z-type configurations of fuel cells, J. Power Sources 269 (2014) 274–283, https://doi.org/10.1016/j.jpowsour.2014.06.136.
[33] Y.Z. Zhang, Y.L. Du, B.C. Sun, Temperature distribution analysis of high-speed railway roadbed in seasonally frozen regions based on empirical model, Cold Reg. Sci. Technol. 114 (0) (2015) 61–72.
[34] Y.Z. Zhang, Study on the Stability of High-Speed Railway Roadbed in Deep Seasonally Frozen Region, Beijing Jiaotong University, Dissertation, 2015.
[35] State Railway Administration, TB 10118-2006 Code for Design for Applications of Geosynthetics on Subgrade of Railway, China Railway Publishing House, Beijing, 2006.

Nomenclature

m: transverse line
$C_{du}(T)$*:* specific heats of the melted $(J\cdot(kg\cdot^{\circ}C)^{-1})$
2*n:* longitudinal line
$C_{df}(T)$*:* specific heats of the frozen soils$(J\cdot(kg\cdot^{\circ}C)^{-1})$
T: Temperature(℃)
L: the latent heat (kJ/kg)
t: time (s)
ρ*:* density $(kg\cdot m^{-3})$
$CU^{'}i,j$*:* homogeneity coefficient
$c_f(T)$*:* specific heat during the phase-transition temperature$(J\cdot(kg\cdot^{\circ}C)^{-1})$
CU: homogeneity matrix
T_r*:* reference temperature (℃)
DCjsymmetry coefficientT_1*:* symmetry coefficientT_1 temperature of the model at the bottom boundary(℃)
DC: coefficient matrix
x: distance(m)
H: enthalpy $(J\cdot m^{-3})$
X: distance from the subgrade center(m)
Tl*:* liquid phase-transition temperature (℃)
Y: the subgrade height(m)
Ts*:* solid phase-transition temperature (℃)
R: evaluation matrix
c: specific heat $(J\cdot(kg\cdot^{\circ}C)^{-1})$
$DC^{'}$*:* temperature symmetry indices
λ*:* thermal conductivity $(W\cdot(m\cdot K)^{-1})$
DC^{z}*:* temperature symmetry indices